Supplementary Information for

Cropland biophysical impacts on land surface temperature show diurnal differences across tropical Africa

Hao Luo[1*], Johannes Quaas[1,2]

[1]Leipzig Institute for Meteorology, Leipzig University, 04103, Leipzig, Germany

[2]German Centre for Integrative Biodiversity Research (iDiv) Halle-Jena-Leipzig, 04103, Leipzig, Germany

[*]Corresponding author. Email: hao.luo@uni-leipzig.de

This supplementary information includes:

Supplementary Figure 1 to Figure 14

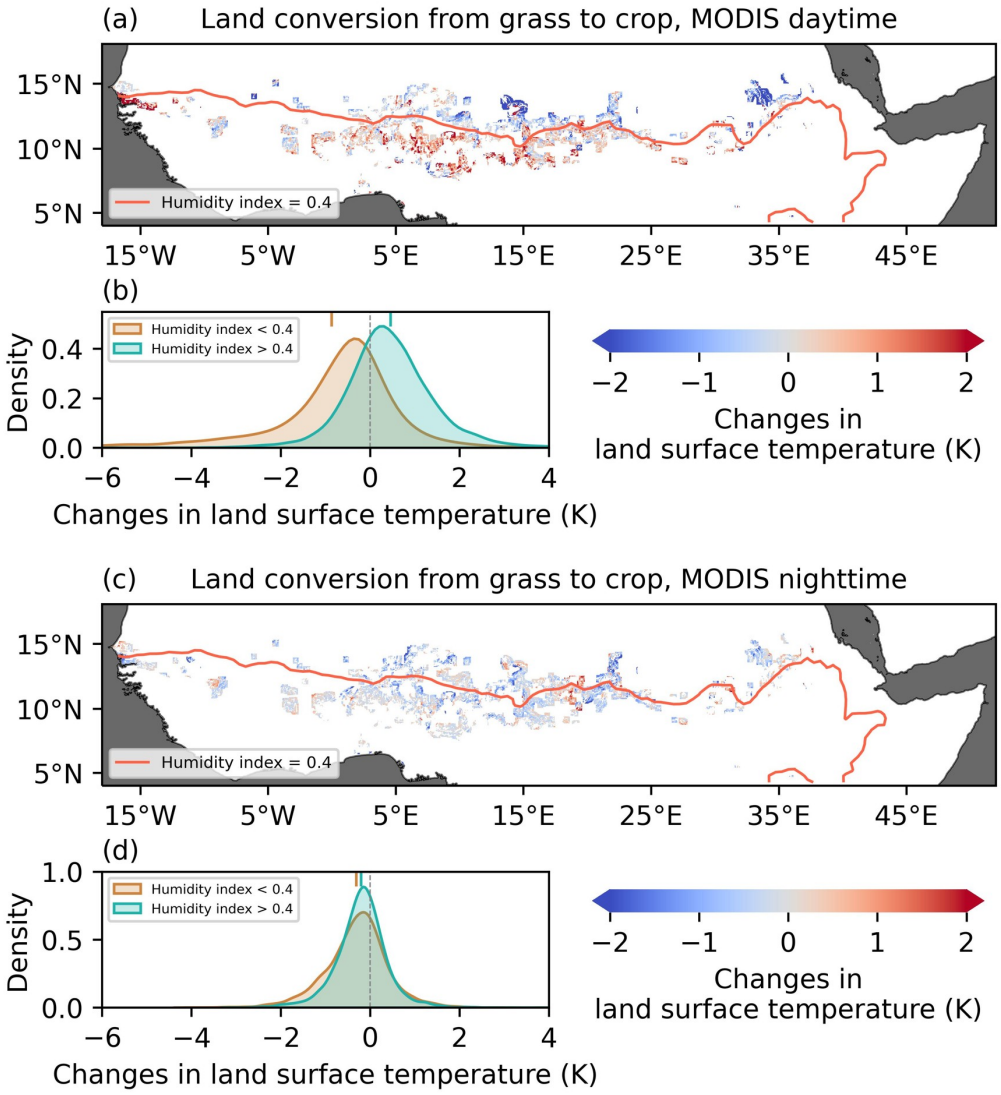

Supplementary Figure 1. Cropland biophysical impacts on daytime and nighttime land surface temperature (*ΔTs*) over tropical Africa. Panels show (a) the map and (b) probability density function (PDF) for daytime, and (c) the map and (d) PDF for nighttime. The pink line in the maps denotes the humidity index (*HI*) = 0.4, which separates the more arid (north) and less arid (south) hydroclimatic regimes. PDFs are also divided into more arid regions (*HI* < 0.4) and less arid regions (*HI* > 0.4). The vertical lines at the top of the PDFs indicate the mean *ΔTs* across all valid moving windows. *ΔTs* is calculated as cropland minus grassland using the space-for-time substitution approach (Methods). *Ts* is derived using 20-year Moderate Resolution Imaging Spectroradiometer (MODIS) observations.

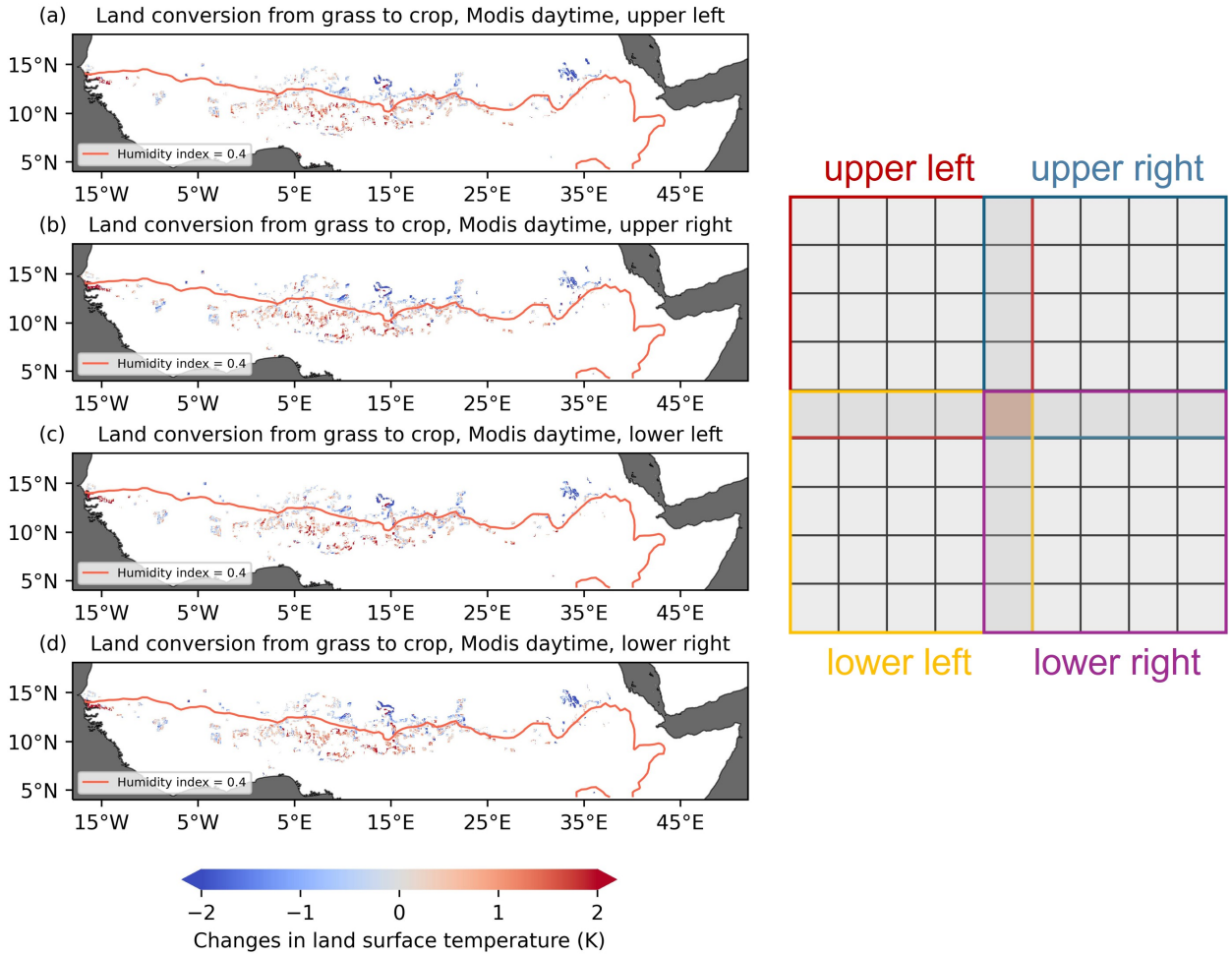

Supplementary Figure 2. Cropland biophysical impacts on daytime land surface temperature (*ΔTs*) over tropical Africa using the four corners of the moving window. Panels (a–d) correspond to Supplementary Figure 1a, but are calculated using the upper left, upper right, lower left, and lower right corners of the moving window, respectively. Illustrations of the four window corners are shown on the right side of the maps.

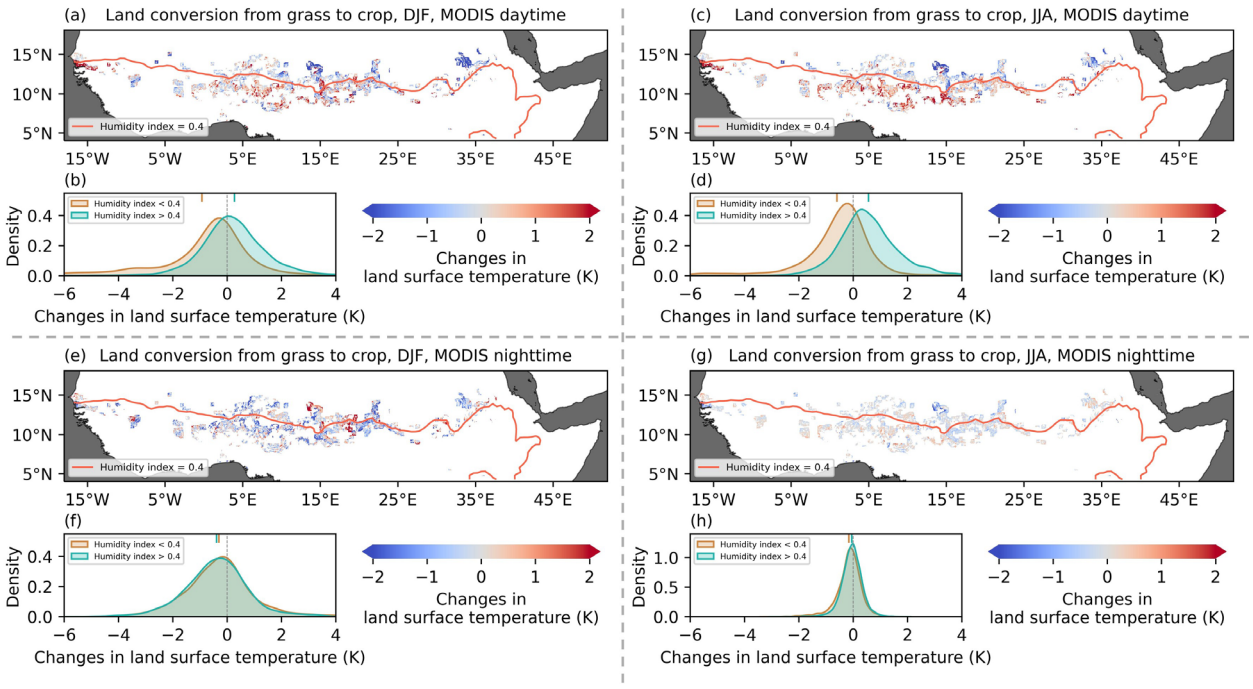

Supplementary Figure 3. Seasonal analyses of cropland biophysical impacts on daytime and nighttime land surface temperature (*ΔTs*) over tropical Africa. Panels (a and b) correspond to Supplementary Figure 1a and b, but are calculated using data only for the dry season (December–January–February, DJF). Panels (c and d) correspond to Supplementary Figure 1a and b, but are calculated using data only for the wet season (June–July–August, JJA). Panels (e and f) correspond to Supplementary Figure 1c and d, but are calculated using data only for the dry season (DJF). Panels (g and h) correspond to Supplementary Figure 1a and b, but are calculated using data only for the wet season (JJA).

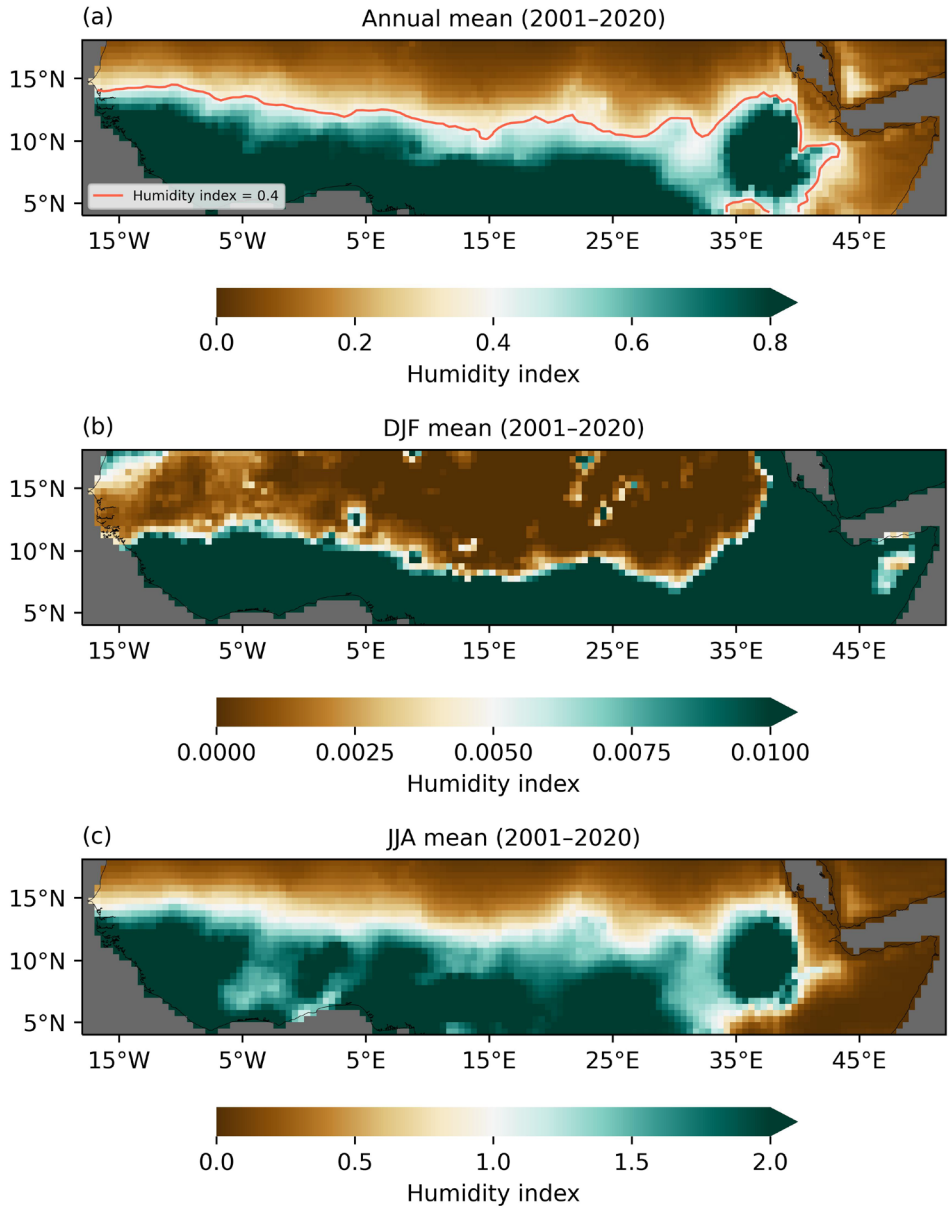

Supplementary Figure 4. Maps of the hydroclimatic conditions over tropical Africa during 2001−2020. The humidity index (*HI*) characterises the background hydroclimatic state and is calculated as the ratio of long-term mean precipitation to potential evapotranspiration, based on monthly data from the CRU TS v4.08 dataset. Panels show the *HI* for (a) the annual period, (b) the dry season (December–January–February, DJF), and (c) the wet season (June–July–August, JJA) during 2001–2020.

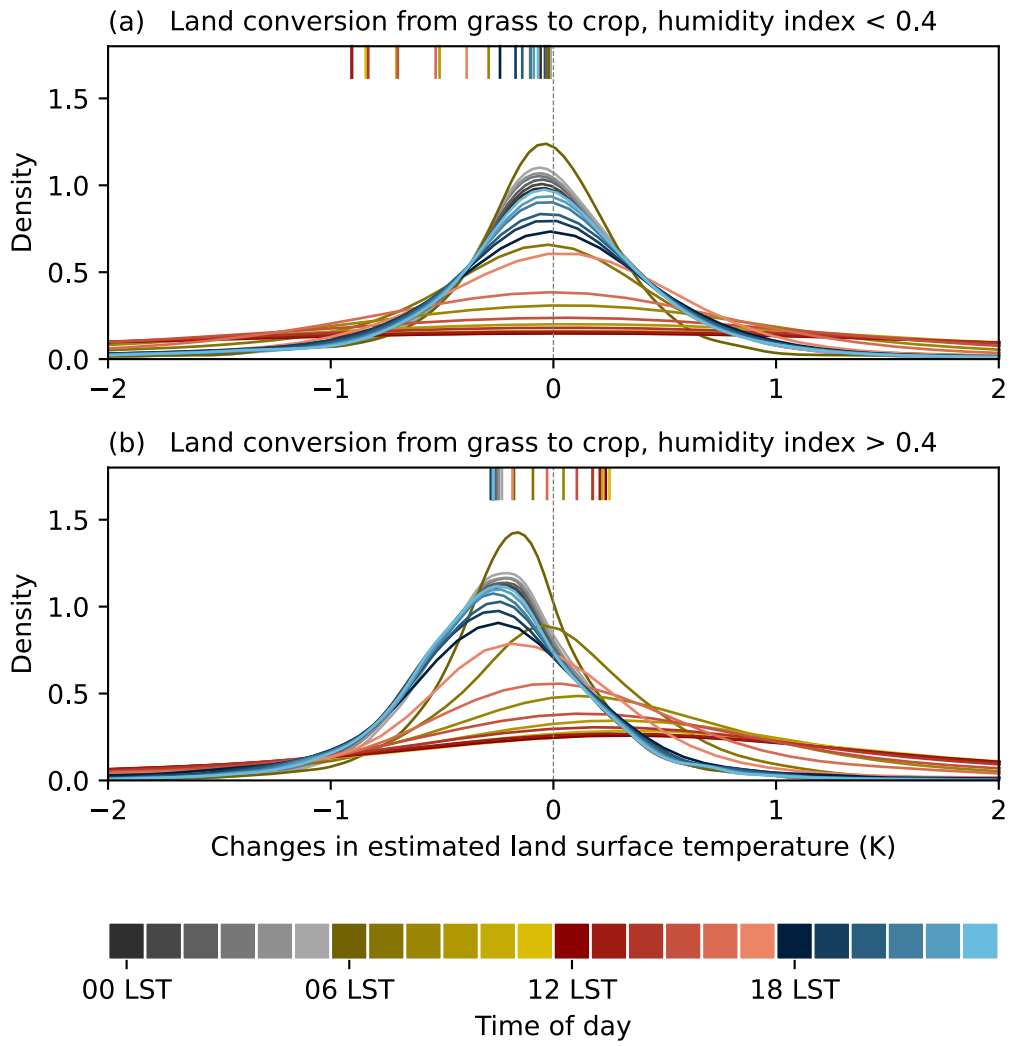

Supplementary Figure 5. Probability density functions (PDFs) of the estimated diurnal cropland biophysical impacts on land surface temperature (*ΔTs*) over tropical Africa. Panels show the PDFs for (a) more arid regions (humidity index, *HI* < 0.4) and (b) less arid regions (*HI* > 0.4). The vertical lines at the top of each panel indicate the mean *ΔTs* across all valid moving windows. Hourly *ΔTs* is estimated using the linear ΔTs attribution framework (Methods).

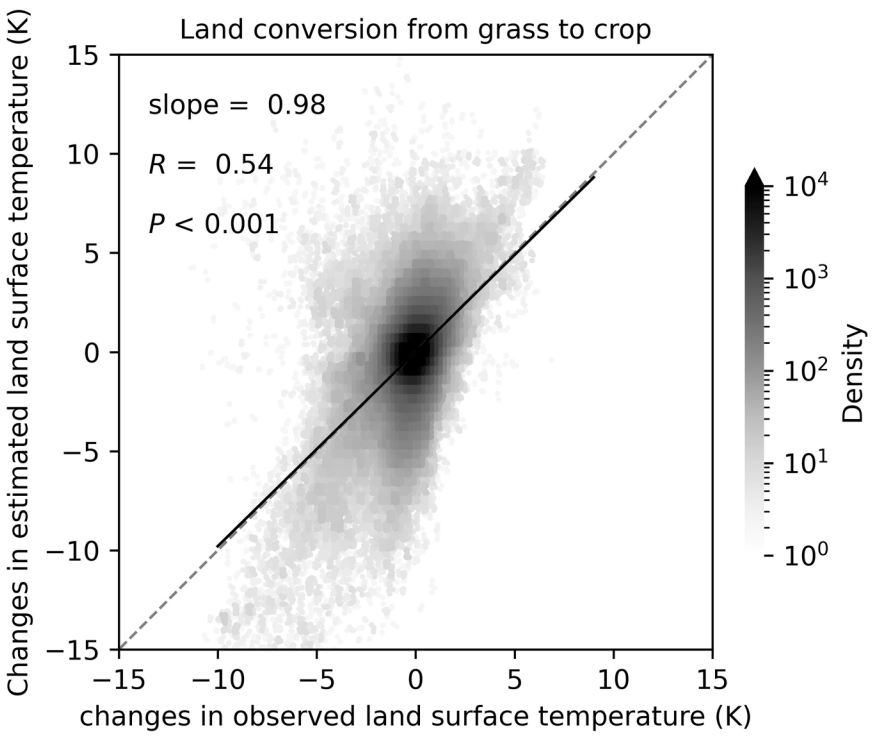

Supplementary Figure 6. Validation of the estimated cropland biophysical impacts on land surface temperature (*ΔTs*) against observations over tropical Africa. The joint histogram shows the relationship between Δ*Ts* from estimations and from observations. Observed Δ*Ts* is calculated as cropland minus grassland using the space-for-time substitution approach (Methods). Estimated Δ*Ts* is derived from the linear *ΔTs* attribution framework (Methods). All datasets are based on 17-year mean hourly Meteosat Second Generation (MSG) geostationary satellite observations. The linear regression is represented by the black lines, with the texts displaying the slope of the linear fit, correlation coefficient (*R*), and *P*-value from a Student's t test.

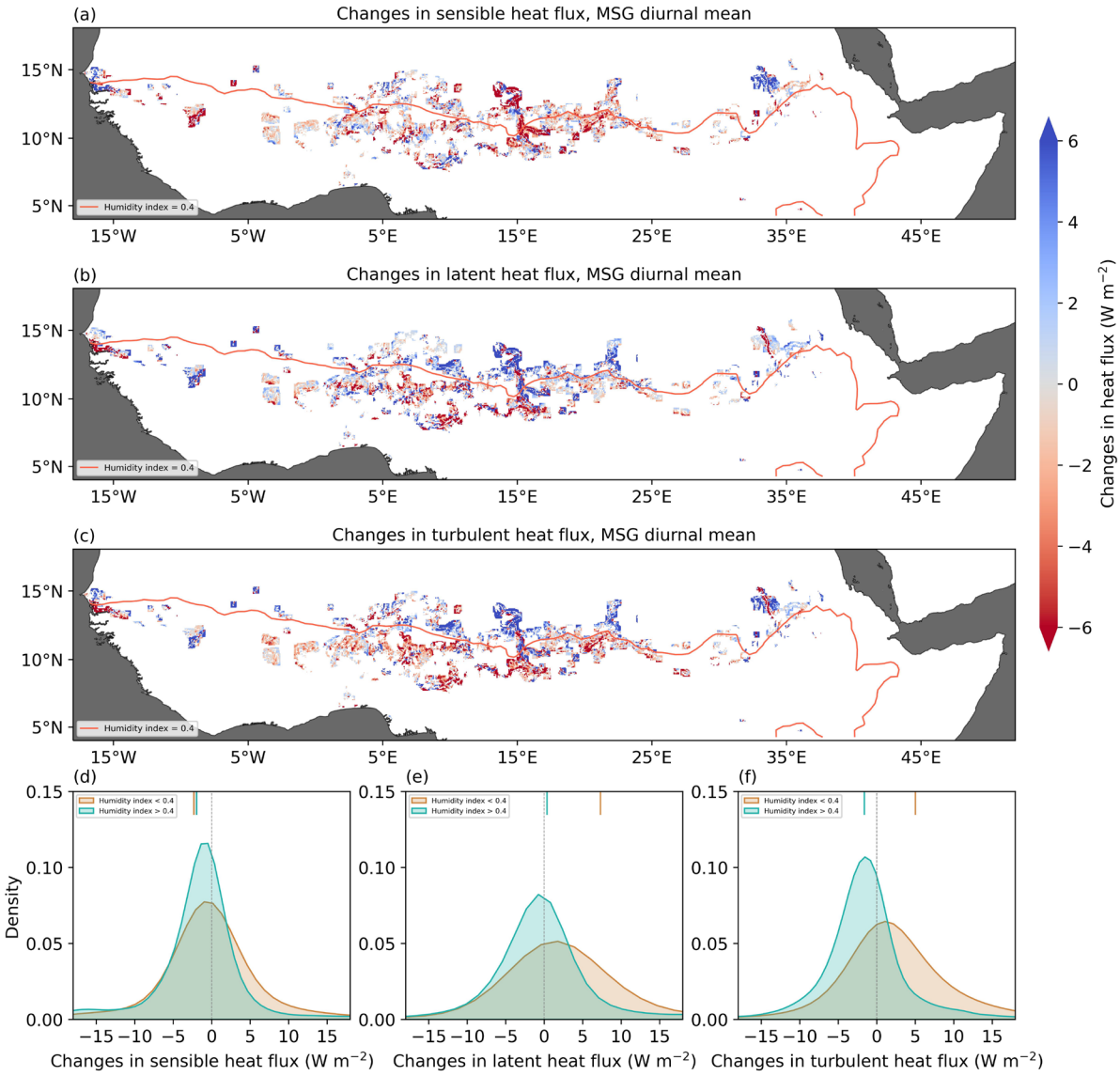

Supplementary Figure 7. Cropland biophysical impacts on sensible heat flux (*ΔH*) and latent heat flux (*ΔLE*) over tropical Africa. Panels show maps of (a) *ΔH*, (b) *ΔLE*, and (c) changes in turbulent heat flux (*ΔH* + *ΔLE*), with the pink line indicating humidity index (*HI*) = 0.4, which separates the more arid and less arid hydroclimatic regimes. Panels (d–f) show the corresponding probability density functions (PDFs) of *ΔH*, *ΔLE*, and *ΔH* + *ΔLE*, respectively. PDFs are also divided into more arid regions (*HI* < 0.4) and less arid regions (*HI* > 0.4). The vertical lines at the top of each panel indicate the means across all valid moving windows. The changes (*Δ*) are calculated as cropland minus grassland using the space-for-time substitution approach (Methods). All datasets are based on 17-year mean Meteosat Second Generation (MSG) geostationary satellite observations.

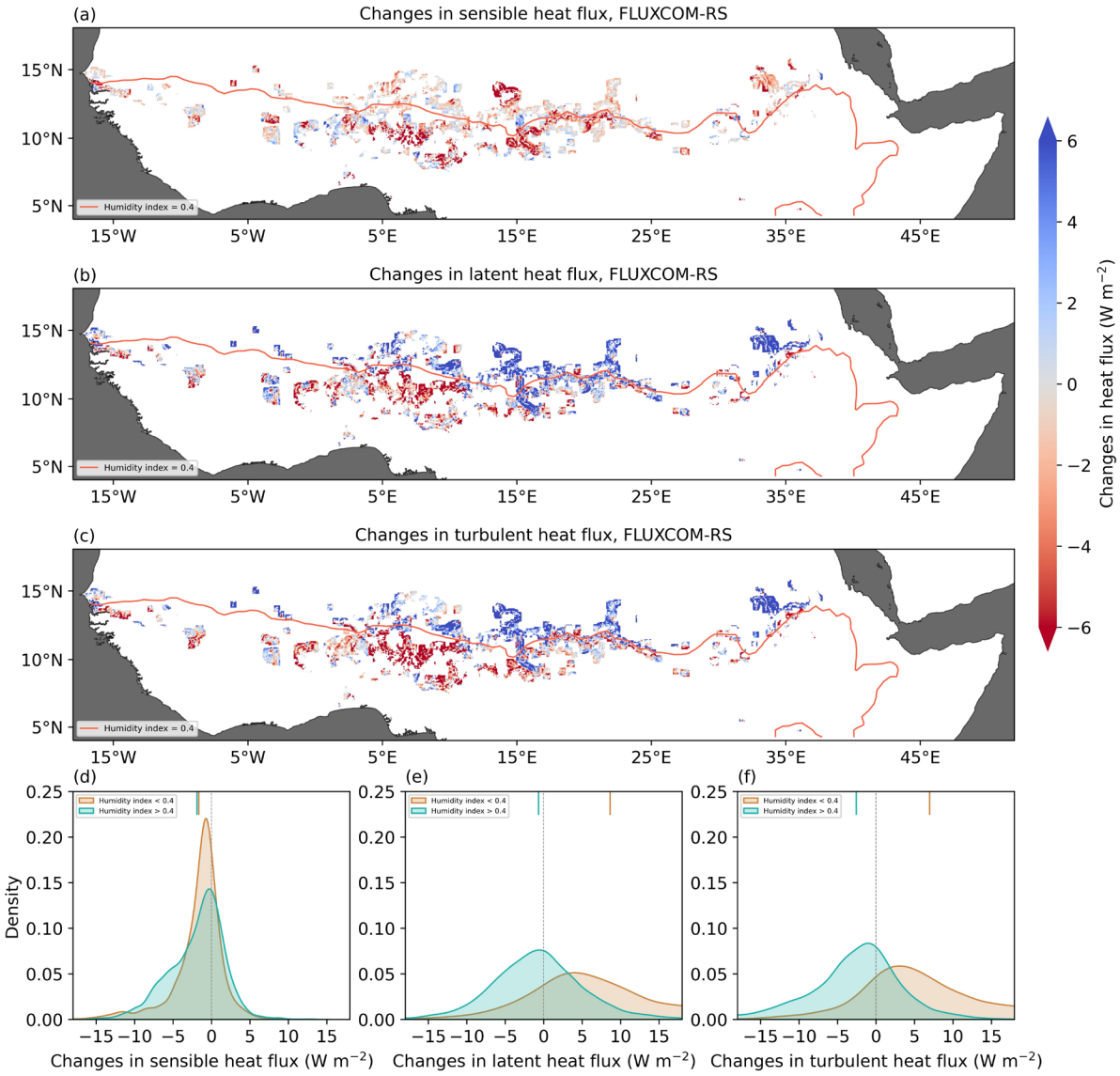

Supplementary Figure 8. Cropland biophysical impacts on sensible heat flux (*ΔH*) and latent heat flux (*ΔLE*) over tropical Africa. As in Supplementary Figure 7, but derived from FLUXCOM-RS data.

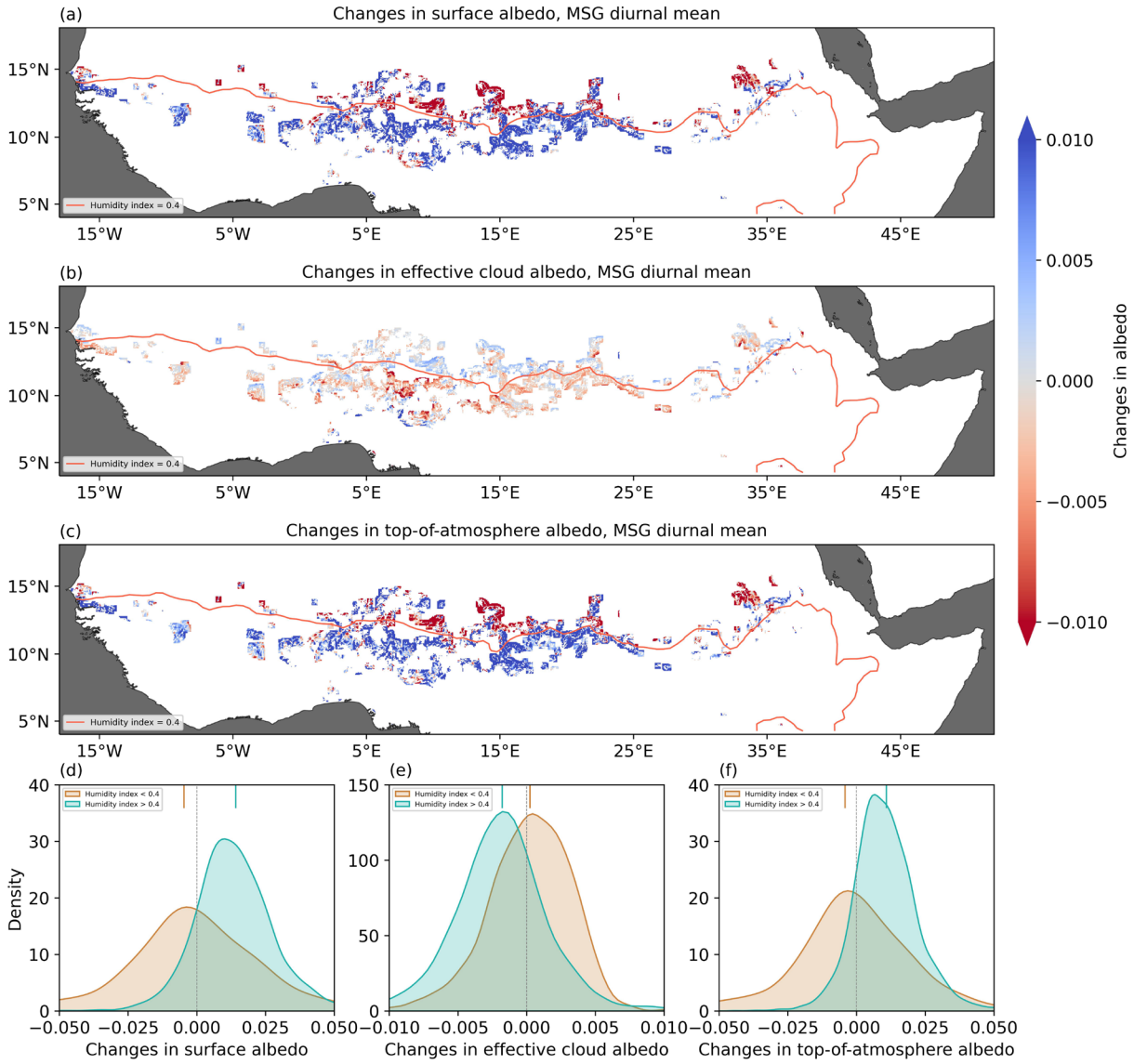

Supplementary Figure 9. Cropland biophysical impacts on albedo over tropical Africa. Panels show maps of (a) changes in surface albedo ($\Delta\alpha$), (b) changes in cloud effective albedo, and (c) changes in top-of-atmosphere albedo, with the pink line indicating humidity index (HI) = 0.4, which separates the more arid and less arid hydroclimatic regimes. Panels (d–f) show the corresponding probability density functions (PDFs) of $\Delta\alpha$, changes in cloud effective albedo, and changes in top-of-atmosphere albedo, respectively. PDFs are also divided into more arid regions (HI < 0.4) and less arid regions (HI > 0.4). The vertical lines at the top of each panel indicate the means across all valid moving windows. The changes (Δ) are calculated as cropland minus grassland using the space-for-time substitution approach (Methods). All datasets are based on 17-year mean Meteosat Second Generation (MSG) geostationary satellite observations.

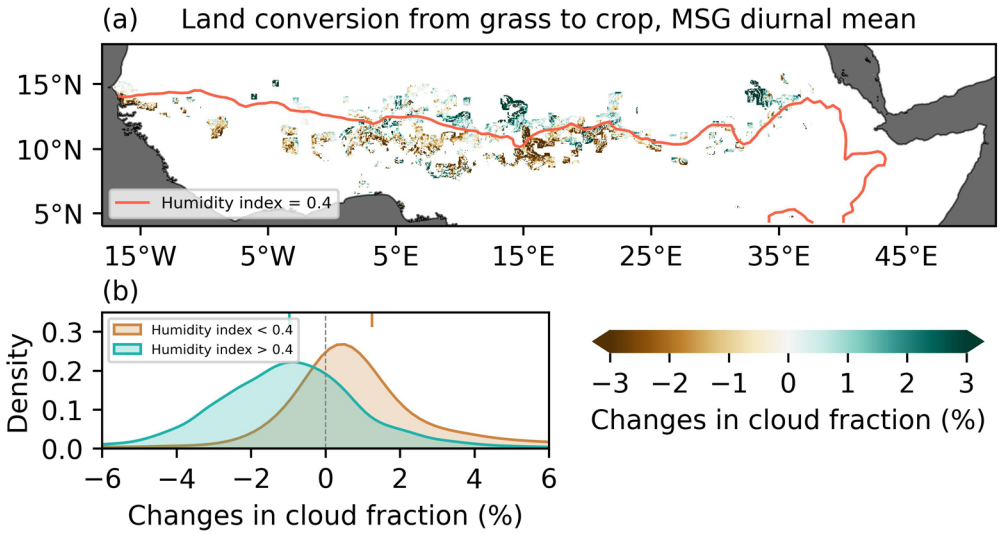

Supplementary Figure 10. Cropland biophysical impacts on cloud fraction over tropical Africa. Panels show (a) the map and (b) the probability density function (PDF) of changes in cloud fraction. The pink line in the map denotes the humidity index (*HI*) = 0.4, which separates the more arid and less arid hydroclimatic regimes. PDFs are also divided into more arid regions (*HI* < 0.4) and less arid regions (*HI* > 0.4). The vertical lines at the top of the PDFs indicate the means across all valid moving windows. Changes in cloud fraction are calculated as cropland minus grassland using the space-for-time substitution approach (Methods). Cloud fraction is derived using 17-year mean Meteosat Second Generation (MSG) geostationary satellite observations.

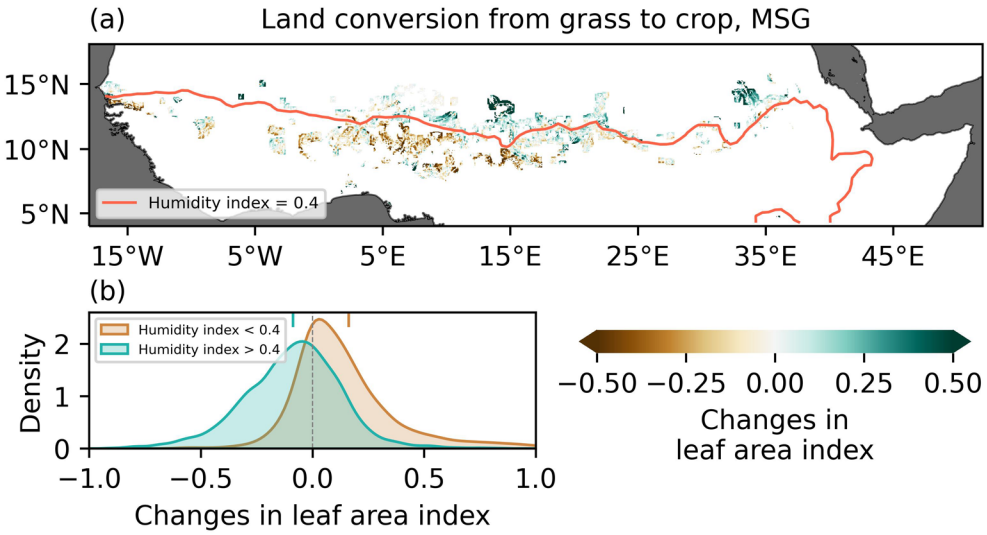

Supplementary Figure 11. Cropland-induced changes in leaf area index (*ΔLAI*) over tropical Africa. Panels show (a) the map and (b) the probability density function (PDF) of *ΔLAI*. The pink line in the map denotes the humidity index (*HI*) = 0.4, which separates the more arid and less arid hydroclimatic regimes. PDFs are also divided into more arid regions (*HI* < 0.4) and less arid regions (*HI* > 0.4). The vertical lines at the top of the PDFs indicate the means across all valid moving windows. *ΔLAI* is calculated as cropland minus grassland using the space-for-time substitution approach (Methods). *LAI* is derived using 17-year mean Meteosat Second Generation (MSG) geostationary satellite observations.

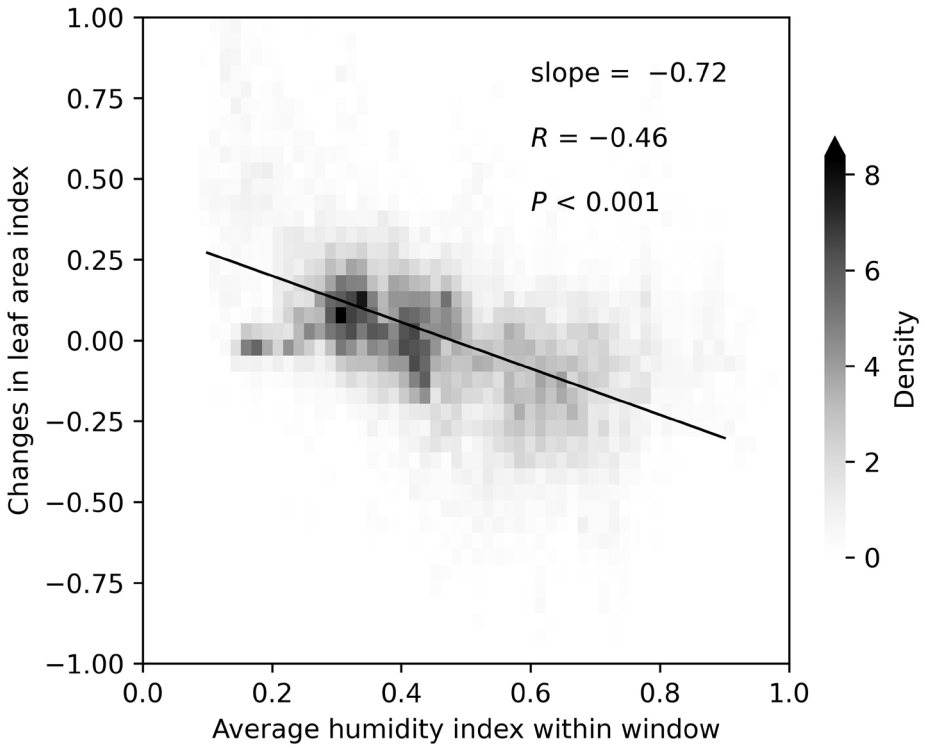

Supplementary Figure 12. Relationship between background humidity index (*HI*) and cropland-induced changes in leaf area index (*ΔLAI*). The joint histogram shows the relationship between average *HI* within each moving window and *ΔLAI*. *ΔLAI* is calculated as cropland minus grassland using the space-for-time substitution approach (Methods). *LAI* is based on 17-year mean Meteosat Second Generation (MSG) geostationary satellite observations. *HI* is calculated as the ratio of long-term mean (2001−2020) annual precipitation amount to potential evapotranspiration, using monthly data from the CRU TS v4.08 datasets. The linear regression is represented by the black line, with the texts displaying the slope of the linear fit, correlation coefficient (*R*), and *P*-value from a Student's t test.

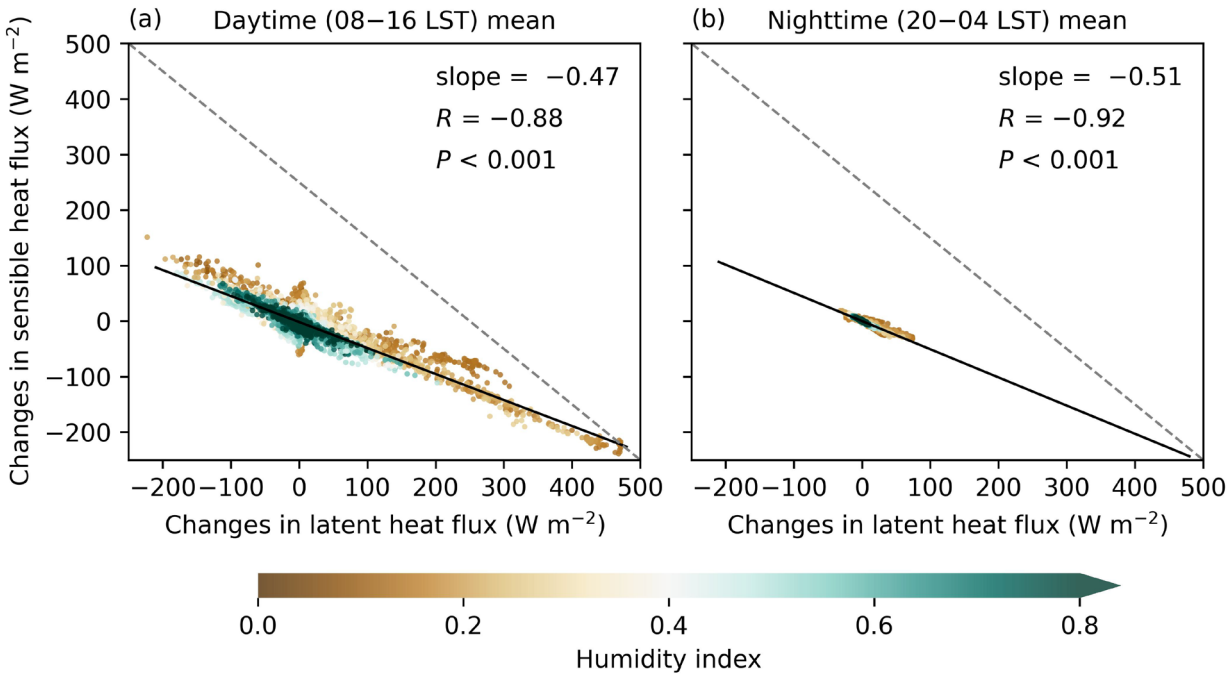

Supplementary Figure 13. Relationships between cropland biophysical impacts on latent heat flux (*ΔLE*) and sensible heat flux (*ΔH*) during daytime and nighttime. Panels illustrate the relationships between *ΔLE* and *ΔH* during (a) daytime (08–16 LST mean) and (b) nighttime (20–04 LST mean). The changes (*Δ*) are calculated as cropland minus grassland using the space-for-time substitution approach (Methods). All datasets are based on 17-year mean hourly Meteosat Second Generation (MSG) geostationary satellite observations. Scatter points are coloured according to the humidity index (*HI*). The linear regressions are represented by the black lines, with the texts displaying the slope of the linear fit, correlation coefficient (*R*), and *P*-value from a Student's t test.

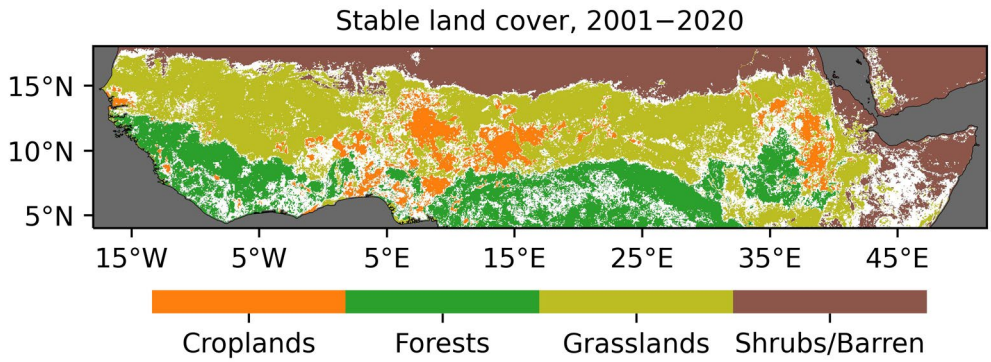

Supplementary Figure 14. Map of the stable land cover over tropical Africa during 2001−2020. Areas classified as stable land cover are defined as pixels where the dominant land cover type remains unchanged throughout 2001–2021. Land cover is derived from the level 3 annual Terra-and-Aqua-combined MODIS land cover type product (MCD12C1, version 061). The International Geosphere–Biosphere Programme (IGBP) classification is adopted for analyses. We define the land cover as: (1) croplands, which includes IGBP class 12 (croplands) and class 14 (cropland natural vegetation mosaic); (2) forests, which includes IGBP classes 1 to 5 (evergreen needleleaf, evergreen broadleaf, deciduous needleleaf, deciduous broadleaf, and mix forests), and IGBP classes 8 and 9 (woody savannas, savannas); (3) grasslands, which includes IGBP classes 10 and 11 (grasslands, permanent wetlands); (4) Shrubs/Barren, which includes IGBP classes 6 and 7 (closed shrublands, open shrublands) and IGBP classes 15 and 16 (permanent snow and ice, barren).